STUDY OF MECHANICAL BEHAVIOR OF DOWEL BAR IN TRANSVERSE JOINTS OF CONCRETE PAVEMENT

(Translation from Proceedings of JSCE, No.683/V-52, August 2001)

Tatsuo Nishizawa

The objective of this study is to develop a mechanical design method for doweled joints. The mechanical behavior of dowel bars is investigated using a mechanical model (PAVE3D) developed for dowel bars in the transverse joints of concrete pavement based on the three-dimensional finite element method. In this model, a dowel bar is divided into two segments that are embedded in concrete connected by a third segment. These two types of segment are modeled by solving for a beam on an elastic foundation and for a three-dimensional beam element, respectively. The model is verified by comparing the predicted strains in the concrete slab and dowel bars with experimental data obtained from loading tests conducted on a model pavement and an actual pavement. The effects of transverse joint structure and subbase stiffness on the stresses in dowel bars and the concrete slab are investigated through numerical simulations with PAVE3D.

Keywords: *concrete pavement, transverse joint, dowel bar, three dimensional finite element method*

Tatsuo Nishizawa is an associate professor in the Department of Civil Engineering at Ishikawa National College of Technology, Japan. He obtained D. Eng. from Tohoku University in 1989. He specializes in structural analysis and evaluation of pavement structures. He is a member of JSCE and chairs the subcommittee of pavement design in JSCE. He is also a member of the committee of rigid pavement design in TRB, USA.

---

1. INTRODUCTION

Transverse joints are one of the weak points of concrete pavements because of the discontinuity they introduce, and as a result such joints are a critical issue in the structural design of concrete pavements. Transverse joints incorporate dowel bars to enhance load transfer across the joint. The geometry and spacing of the dowel bars are determined empirically in the Japanese design manual [1]. A survey in Japan has shown that the concrete pavement of many roads with heavy traffic suffers from longitudinal cracks that have initiation points at transverse joints under wheel paths [2]. Another study has shown that some dowel bars fail at opening of the transverse joints [3]. These findings suggest that the current design of dowel bars for transverse joints might be inappropriate. Therefore, there is a desire to establish a rational design method for doweled joints based on mechanical analysis.

Finite element (FE) models based on the plate theory have been employed to analyze the mechanical behavior of concrete slabs at transverse joints, including dowel action [4,5,6,7,8]. In these models, the function of the dowel bar at the joint is represented by a shear spring and/or a beam element. The authors have previously proposed a refined model for dowel bar function, where a dowel bar is divided into a segment between the concrete slabs and two opposing segments embedded in the concrete [9,10]. These two types of segment are modeled with a beam element and local displacement elements, respectively. This model has been employed by other researchers using FE analysis and its validity was confirmed [11].

The three-dimensional finite element method (3DFEM) has been recognized as a powerful tool in the analysis and design of pavement structures. Recently, two symposiums relating to this subject were held in the USA [12, 13]. The use of 3DFEM allows pavement engineers to compute displacements and stresses not only in the concrete slabs themselves, but also in the subbase and subgrade that cannot be dealt with using a 2D slab model. In applying 3DFEM to concrete pavements, the model used for load transfer across the joint remains of great significance [14,15]. In this study, we develop a 3DFEM code for concrete pavements that includes dowel bar function at transverse joints as well as the opening-closure phenomenon at the interface between concrete slab and subbase. This 3DFEM code for pavement structures is named PAVE3D, and consists of an FEM solver and pre/post processors. We incorporate the refined dowel model into PAVE3D and investigate the effects of dowel bar geometry and spacing, as well as subbase stiffness, on stresses in the dowel bar and the concrete slab.

2. STRUCTURAL MODEL

2.1 3D FE Model for Pavement

Figure 1 shows the pavement structure considered in PAVE3D. This pavement consists of elastic layers that represent the concrete slab, the subbase, and the subgrade, all of which are divided into solid elements. The interface between the concrete slab and the subbase is modeled using a general interface element. The dowel bar element is included in the joint interface element.

Each layer has a finite horizontal extent and displacement in the normal direction on each edge is fixed; other displacements are free. This boundary condition is not applied to the top layer. All displacements are fixed at nodes on the bottommost surface of the structure. Loads are applied on the surface both vertically and horizontally as uniformly distributed rectangular loads. The temperature distribution is specified as a linear function of z for each layer.

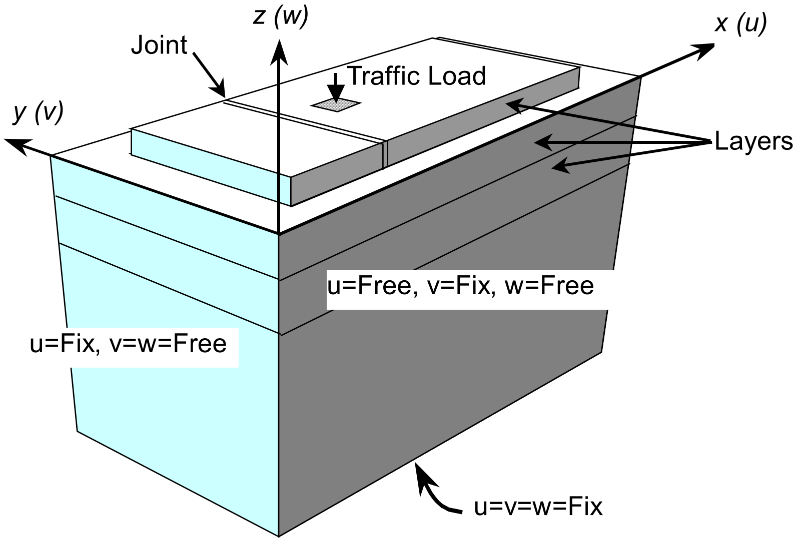

Figure 1 Structural Model of Pavement

2.2 Solid Elements

The eight-node solid element shown in Figure 2 is employed in this study. Displacements in the solid element are expressed with the following shape functions [16]:

$$\begin{Bmatrix} u \\ v \\ z \end{Bmatrix} = \sum_{i=0}^{7} \begin{bmatrix} N_i & 0 & 0 \\ 0 & N_i & 0 \\ 0 & 0 & N_i \end{bmatrix} \begin{Bmatrix} u_i \\ v_i \\ w_i \end{Bmatrix} \qquad (1)$$

where,

$u,\ v,\ w$ = displacements in x, y, and z directions, respectively, within an element,

$u_i,\ v_i,\ w_i$ = displacements in x, y, and z directions, respectively, at node i, and

$N_i = \frac{1}{8}(1+\xi_i\xi)(1+\eta_i\eta)(1+\zeta_i\zeta)$.

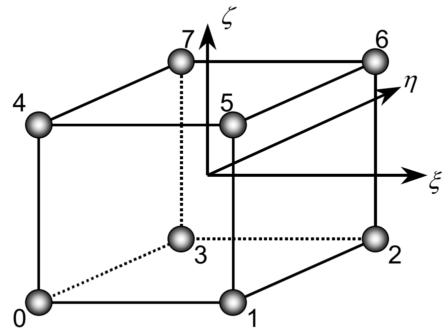

Figure 2 Eight-Node Solid Element

2.3 Interface Elements

In order to deal with bonding at the interface between the concrete slab and the subbase as well as aggregate interlocking at cracks or joints, we have developed the general interface element shown in Figure 3. This element consists of two planes: Plane 0 and Plane 1. It is assumed that stresses proportional to the differential displacement between the planes are transferred, as expressed by:

$$\begin{Bmatrix} \Delta f_{x'} \\ \Delta f_{y'} \\ \Delta f_{z'} \end{Bmatrix} = \begin{bmatrix} k_{x'} & 0 & 0 \\ 0 & k_{y'} & 0 \\ 0 & 0 & k_{z'} \end{bmatrix} \begin{Bmatrix} \Delta u' \\ \Delta v' \\ \Delta w' \end{Bmatrix} \quad or \quad \{\Delta \mathbf{f}'\} = [\mathbf{k}']\{\Delta \mathbf{d}'\} \tag{2}$$

where,

$f_{x'}$, $f_{y'}$, $f_{z'}$ = forces in x', y', and z' directions, respectively, within a plane,

u', v', w' = displacements in x', y', and z' directions, respectively, within an element, and

$k_{x'}$, $k_{y'}$, $k_{z'}$ = spring coefficients in x', y', and z' directions, respectively.

Δ indicates the differential displacement or force between Plane 0 and Plane 1. Using Equation (2) and applying the principle of virtual work to the element, the stiffness matrix can be obtained [17].

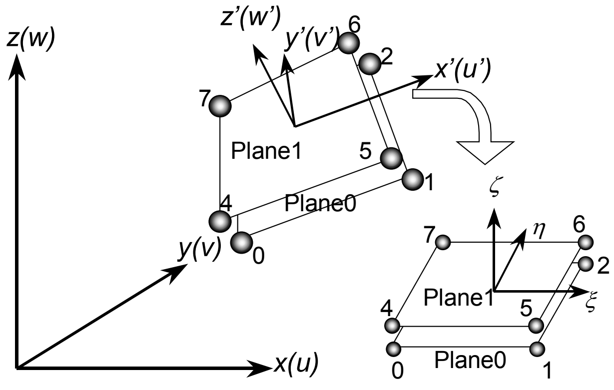

Figure 3 General Interface Element

2.4 Spring Coefficients

In a concrete pavement, portions of the bottom surface of the concrete slab may separate from the top surface of the subbase if curling deformation occurs due to a temperature gradient in the concrete slab. In order to take into account this phenomenon, the spring coefficients of the interface element are assumed to be a function of differential displacement Δu as follows:

$$k = \begin{cases} k & \Delta u < 0 \\ \dfrac{k}{2}\left\{\cos\left(\dfrac{\Delta u \pi}{\Delta_0}\right) + 1.0\right\} & 0 \le \Delta u \le \Delta_0 \\ 0 & \Delta_0 < \Delta u \end{cases} \tag{3}$$

If the spring coefficients change rapidly with displacement, there will be no reasonable converging solutions. Therefore, a transition range ($0 \le \Delta u \le \Delta_0$) is introduced in Equation (3). In this study, the value of Δ_0 is determined to be 0.0001 mm on the basis of some trial calculations. If an interface element is used to model a crack, $k_{x'}$ and $k_{y'}$ represent the shear and torsional transfer while $k_{z'}$ represents moment and axial load transfer across the crack.

2.5 Non Linear Analysis

The global stiffness equation for the 3DFEM model with solid and interface elements can be written as follows:

$$(\mathbf{K}_s + \mathbf{K}_j) \cdot \mathbf{d} = \mathbf{f}_p + \mathbf{f}_v + \mathbf{f}_t \tag{4}$$

where,

$\mathbf{K}_s$: stiffness matrix of 8-node solid element,

$\mathbf{K}_j$: stiffness matrix of interface element,

$\mathbf{d}$: displacement vector,
$\mathbf{f}_p$: external load vector,
$\mathbf{f}_v$: self-weight load vector, and
$\mathbf{f}_t$: temperature load vector.

If the stiffness matrix of the interface element is a function of displacement, Equation (4) becomes nonlinear. We solve the equation using the Newton-Raphson method. If the displacement vector at iteration (i-1), $\mathbf{d}^{i-1}$, is known, the residual forces of Equation (4) can be computed by:

$$\Delta\mathbf{r} = \mathbf{f}_p + \mathbf{f}_v + \mathbf{f}_t - \left(\mathbf{K}_s + \mathbf{K}_j\right)\cdot \mathbf{d}^{i-1} \tag{5}$$

The correction vector for the displacement, $\Delta\mathbf{d}^{i-1}$, is estimated by solving the following equation:

$$\Delta\mathbf{r} = \left(\mathbf{K}_s + \mathbf{K}_j\right)\cdot \Delta\mathbf{d}^{i-1} \tag{6}$$

Then, the new displacement vector for the next iteration can be obtained by $\mathbf{d}^i = \mathbf{d}^{i-1} + \Delta\mathbf{d}^{i-1}$. This process is repeated until a certain degree of convergence is reached.

3. DOWEL BAR MODEL

3.1 Basic Concept

As already mentioned, the dowel bar is divided into three segments: one segment between the

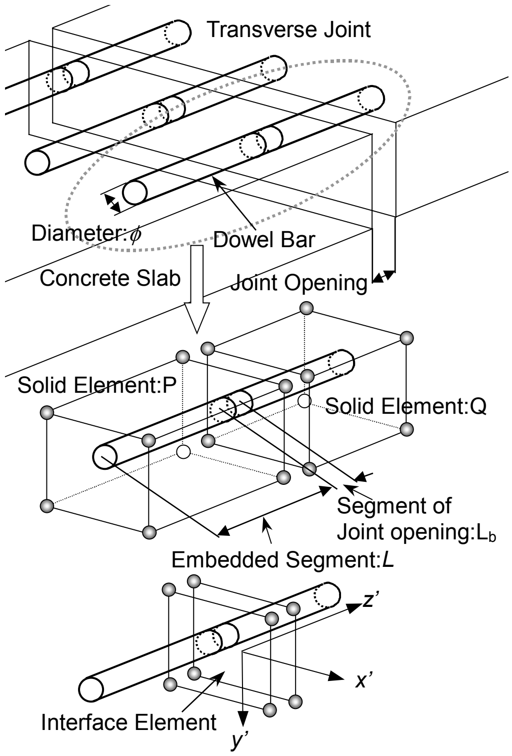

Figure 4 Dowel Bar Element

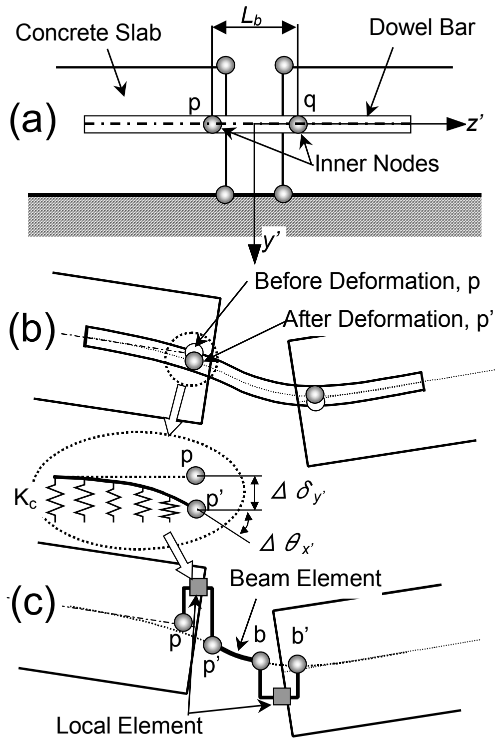

Figure 5 Displacement of Dowel Bar Element

slabs and one segment embedded in the concrete of each slab. This is shown in Figure 4. The between-slab segment is represented by a beam element that is in turn connected to two solid elements (elements P and Q) at the two nodes. These nodes are located within the elements and are defined as inner nodes, p and q, as shown in Figure 5. Displacements at inner node p can be expressed in terms of the nodal displacements of Element P as:

$$\begin{Bmatrix} u' \\ v' \\ w' \\ \theta_{x'} \\ \theta_{y'} \\ \theta_{z'} \end{Bmatrix}^p = \sum_{i=0}^{7} \begin{bmatrix} N_i & 0 & 0 \\ 0 & N_i & 0 \\ 0 & 0 & N_i \\ 0 & -\dfrac{\partial N_i}{\partial z'} & 0 \\ \dfrac{\partial N_i}{\partial z'} & 0 & 0 \\ 0 & 0 & 0 \end{bmatrix}^p \cdot \begin{Bmatrix} u_i' \\ v_i' \\ w_i' \end{Bmatrix}^P \quad or \quad \{d^p\} = [N_i] \cdot \{d^P\} \tag{7}$$

where,

$\theta_{x'}$, $\theta_{y'}$, $\theta_{z'}$ = rotations for the x', y', and z' axes, respectively.

Superscripts p and P indicate components relating to inner node p and Element P, respectively.

Inner node p moves as the concrete slab deforms. The position of node p after deformation is not identical with its original position in Element P, because of local deformation of the surrounding concrete. This situation is illustrated in Figure 5(b). The local deformation is represented by a local element inserted between nodes p and p'. The stiffness of the local element is expressed as the solution of the beam on an elastic foundation, as follows:

$$\begin{Bmatrix} \Delta v' \\ \Delta \theta_{x'} \end{Bmatrix} = a_0 \begin{bmatrix} a_1 & -a_2 \\ -a_2 & a_3 \end{bmatrix} \cdot \begin{Bmatrix} \Delta f_{y'} \\ \Delta m_{x'} \end{Bmatrix} \tag{8}$$

in plane y'-z', where,

$$a_0 = \frac{2\beta^2}{k(S^2 - s^2)},\ a_1 = \frac{1}{\beta}(SC - sc),\ a_2 = (S^2 + s^2),\ a_3 = 2\beta(SC + sc),\ \beta = \sqrt[4]{\frac{K_c \phi}{4 E_d I_d}}$$

K_c = interaction spring coefficient of surrounding concrete,

ϕ = diameter of dowel bar,

$E_d I_d$ = bending rigidity of dowel bar,

$s = \sin(\beta L)$, $c = \cos(\beta L)$, $S = \sinh(\beta L)$, $C = \cosh(\beta L)$,

L = embedded length of dowel bar,

$f_{y'}$ = shear force in y' direction, and

$m_{x'}$ = moment for x' axis.

In plane z'-x', it becomes:

$$\begin{Bmatrix} \Delta u' \\ \Delta \theta_{y'} \end{Bmatrix} = a_0 \begin{bmatrix} a_1 & a_2 \\ a_2 & a_3 \end{bmatrix} \cdot \begin{Bmatrix} \Delta f_{x'} \\ \Delta m_{y'} \end{Bmatrix} \tag{9}$$

where

$f_{x'}$ = shear force in x' direction, and

$m_{y'}$ = moment for y' axis.

Combining Equations (8) and (9), one can obtain:

$$\{\Delta f\} = [A^P]\{\Delta d\} \tag{10}$$

where,

$\{\Delta f\} = \{f^p\} - \{f^{p'}\}$,

$\{\Delta d\} = \{d^p\} - \{d^{p'}\}$,

$\{f\} = \{f_{x'} \ f_{y'} \ f_{z'} \ m_{x'} \ m_{y'} \ m_{z'}\}^t$ and

$\{d\} = \{u' \ v' \ w' \ \theta_{x'} \ \theta_{y'} \ \theta_{z'}\}^t$.

$[A^P]$ is a matrix of size 6 by 6 and its non-zero components are:

$$A_{00}^P = A_{11}^P = a_4 a_3,\ A_{33}^P = A_{44}^P = a_4 a_1,\ A_{04}^P = -A_{13}^P = -a_4 a_2,\ a_4 = \frac{2\beta^2 E_s I_s}{C^2 + c^2}$$

Applying the theory of virtual work to the local element between nodes p and p', one obtains the following relationship:

$$\begin{Bmatrix} f^p \\ f^{p'} \end{Bmatrix} = \begin{bmatrix} A^P & -A^P \\ -A^P & A^P \end{bmatrix} \cdot \begin{Bmatrix} d^p \\ d^{p'} \end{Bmatrix} \tag{11}$$

For the local element between nodes q and q', it becomes:

$$\begin{Bmatrix} f^q \\ f^{q'} \end{Bmatrix} = \begin{bmatrix} A^Q & -A^Q \\ -A^Q & A^Q \end{bmatrix} \cdot \begin{Bmatrix} d^q \\ d^{q'} \end{Bmatrix} \tag{12}$$

The stiffness equation for the three dimensional beam element between nodes p' and q' is [18]:

$$\begin{Bmatrix} f^{p'} \\ f^{q'} \end{Bmatrix} = \begin{bmatrix} S_{00} & S_{01} \\ S_{10} & S_{11} \end{bmatrix} \cdot \begin{Bmatrix} d^{p'} \\ d^{q'} \end{Bmatrix} \tag{13}$$

Superimposing all the equations mentioned above, the stiffness equation for the dowel bar as a whole becomes:

$$\begin{Bmatrix} f^p \\ f^{p'} \\ f^{q'} \\ f^q \end{Bmatrix} = \begin{bmatrix} A^P & -A^P & 0 & 0 \\ -A^P & A^P + S_{00} & S_{01} & 0 \\ 0 & S_{10} & A^Q + S_{11} & -A^Q \\ 0 & 0 & -A^Q & A^Q \end{bmatrix} \cdot \begin{Bmatrix} d^p \\ d^{p'} \\ d^{q'} \\ d^q \end{Bmatrix} \tag{14}$$

Considering

$$\begin{Bmatrix} f^{p'} \\ f^{q'} \end{Bmatrix} = \begin{Bmatrix} 0 \\ 0 \end{Bmatrix}, \tag{15}$$

one obtains the stiffness matrix of the dowel bar element as follows:

$$\begin{Bmatrix} f^p \\ f^q \end{Bmatrix} = \begin{bmatrix} K_{00}^d & K_{01}^d \\ K_{10}^d & K_{11}^d \end{bmatrix} \cdot \begin{Bmatrix} d^p \\ d^q \end{Bmatrix} \tag{16}$$

where,

$$\begin{bmatrix} K_{00}^d & K_{01}^d \\ K_{10}^d & K_{11}^d \end{bmatrix} = \begin{bmatrix} A^P & 0 \\ 0 & A^Q \end{bmatrix} \left[\begin{bmatrix} I & 0 \\ 0 & I \end{bmatrix} - \begin{bmatrix} A^P + S_{00} & S_{01} \\ S_{10} & A^Q + S_{11} \end{bmatrix}^{-1} \begin{bmatrix} A^P & 0 \\ 0 & A^Q \end{bmatrix} \right] \tag{17}$$

and $[I]$ is a unit matrix of size 6 by 6. On the other hand, if the width of the joint is very small, the beam element between nodes p' and q' is removed and the two local elements are directly connected at a node. In this case, the stiffness matrix of the dowel bar element becomes:

$$\begin{bmatrix} K_{00}^{d} & K_{01}^{d} \\ K_{10}^{d} & K_{11}^{d} \end{bmatrix} = \begin{bmatrix} A^{P} & 0 \\ 0 & A^{Q} \end{bmatrix} \left[\begin{bmatrix} I & 0 \\ 0 & I \end{bmatrix} - \begin{bmatrix} A^{P} \cdot B \cdot A^{P} & A^{P} \cdot B \cdot A^{Q} \\ A^{Q} \cdot B \cdot A^{P} & A^{Q} \cdot B \cdot A^{Q} \end{bmatrix} \right] \tag{18}$$

where,

$[B] = \left[A^{P} + A^{Q}\right]^{-1}$

Using Equation (7), Equations (17) and (18) can be converted into a stiffness equation expressed in terms of the displacement vectors of the solid elements, P and Q:

$$\begin{Bmatrix} f^{P} \\ f^{Q} \end{Bmatrix} = \begin{bmatrix} N^{p} & 0 \\ 0 & N^{q} \end{bmatrix}^{t} \cdot \begin{bmatrix} K_{00}^{d} & K_{01}^{d} \\ K_{10}^{d} & K_{11}^{d} \end{bmatrix} \cdot \begin{bmatrix} N^{p} & 0 \\ 0 & N^{q} \end{bmatrix} \cdot \begin{Bmatrix} d^{P} \\ d^{Q} \end{Bmatrix} \tag{19}$$

Since Equation (19) is formulated in the local coordinates of the interface element, it should be moved into global coordinates using the coordinate transfer matrix.

4. VERIFICATION OF DOWEL BAR MODEL

4.1 Model Pavement

In order to experimentally investigate the mechanical behavior of a dowel bar, a model pavement consisting of a 100 mm-thick concrete slab on a granular base was constructed in a laboratory, as shown in Figure 6. Two types of transverse joint, consisting of dowel bars 23 mm and 11 mm in diameter, were incorporated. Strains in the dowel bars produced by a vertical load applied at the transverse joint edge were measured with gauges attached to the surface of the dowel bars. The experiment was

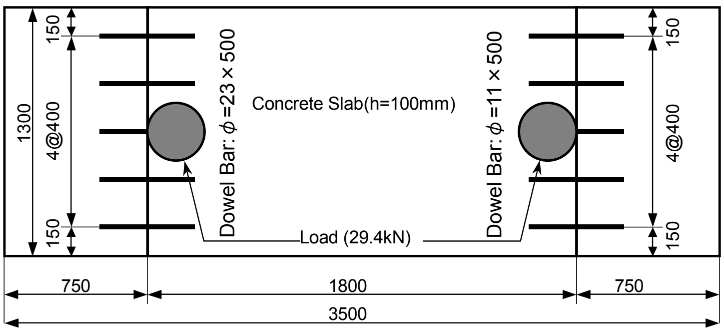

Figure 6 Overview of Model Pavement

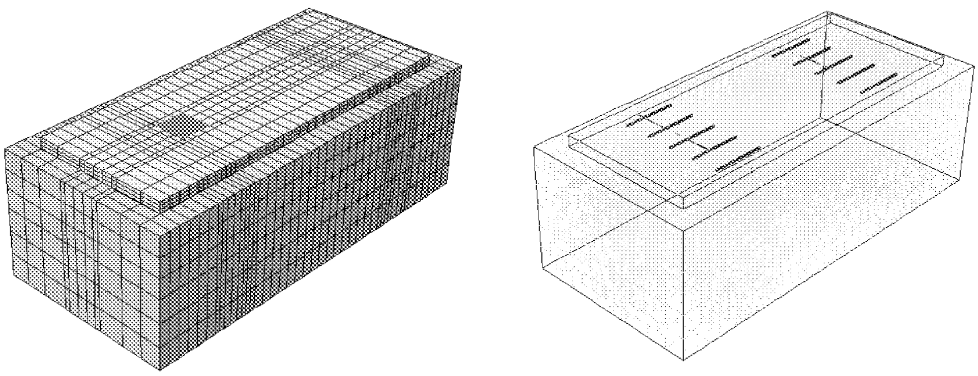

Figure 7 Mesh and Dowel Bar Arrangement for Analysis of Model Pavement

also simulated using PAVE3D. The mesh used in the analysis is shown in Figure 7, and input data used in the analysis is presented in Table 1. The interaction spring coefficient, K_c, varied from 100 GN/m^3 to 400 GN/m^3 according to Yoder et al. [19]

Table 1 Input Data for Analysis of Loading Tests on Model Pavement

Item [Symbol]	Value	Item [Symbol]	Value
Elastic Modulus of Concrete [E_c]	24,000 MPa	Diameter of Dowel Bar [ϕ]	11 and 23 mm
Poisson's Ratio of Concrete [μ_c]	0.2	Length of Dowel Bar [L_d]	500 mm
Thickness of Concrete Slab [h_c]	100 mm	Elastic Modulus of Dowel Bar [E_d]	210,000 MPa
Elastic Modulus of Foundation [E_b]	50 MPa	Poisson's Ratio of Dowel Bar [μ_d]	0.3
Poisson's Ratio of Foundation [μ_b]	0.35	Interaction Spring Constant between Dowel Bar andConcrete [K_c]	100, 200, and 400 GN/m^3
Thickness of Foundation [h_b]	1200 mm		

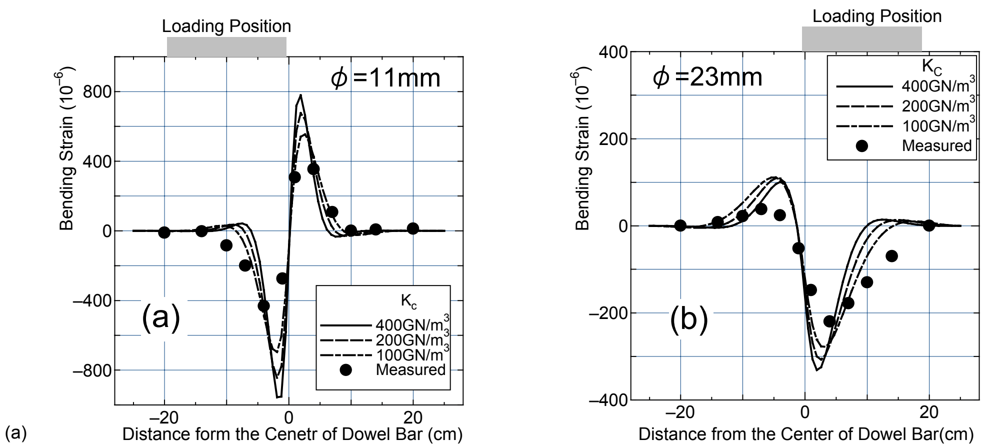

Figure 8 Strain Distributions in Dowel Bars; (a) ϕ=11 mm; (b) ϕ =23 mm

Figure 8 compares the predicted bending strains in a dowel bar immediately below the load with the measured values. In the case of the 11 mm-diameter dowel bar, the measured strain distribution is nearly symmetrical with respect to the center of the dowel bar, because shear load transfer was predominant. On the other hand, in the case of the 23 mm-diameter dowel bar, strains in the loaded side were much larger than those in the unloaded side, because the contribution of dowel bending action to load transfer was significant. Strains computed by PAVE3D indicate a similar tendency to the measured ones. The computed strains increased by 25% to 30% as K_c increased from 100GN/m^3 to 400GN/m^3.

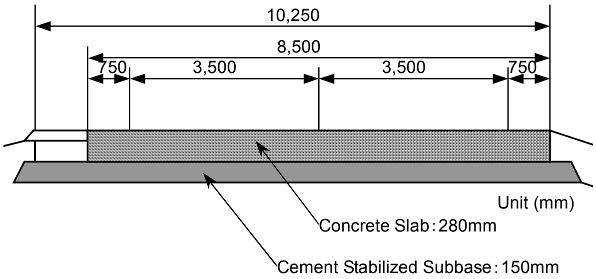

Figure 9 Overview of Actual Pavement

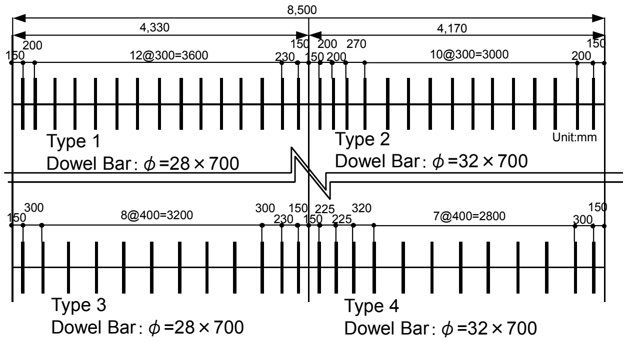

Figure10 Arrangement of Dowel Bars in Transverse Joints

4.2 Actual Pavement

A loading test was conducted on a concrete pavement of an expressway to investigate the mechanical behavior of transverse joints in actual use. Figure 9 shows a section of the pavement , which consists of 280 mm-thick concrete slabs on a 150 mm-thick cement-stabilized subbase. Four types of transverse joint were constructed so as to study the effects of dowel bar diameter and spacing, as shown in Figure 10. Strain gauges were attached to the top and bottom surfaces of the third and fourth dowel bars from the longitudinal edge with an interval of 30 mm. And another strain gauges were attached to the top surface of the slab along the transverse joint edge at intervals of 200 mm. A large truck with tandem rear axle (98 kN per axle) was used to apply a load at the transverse joint edge. The strains in the dowel bars and slabs were measured as the axle approached the joint edge. The loading test was simulated by PAVE3D using the mesh shown in Figure 11 and with the input data presented in Table 2. In this analysis, K_c of 400 GN/m^3 was used.

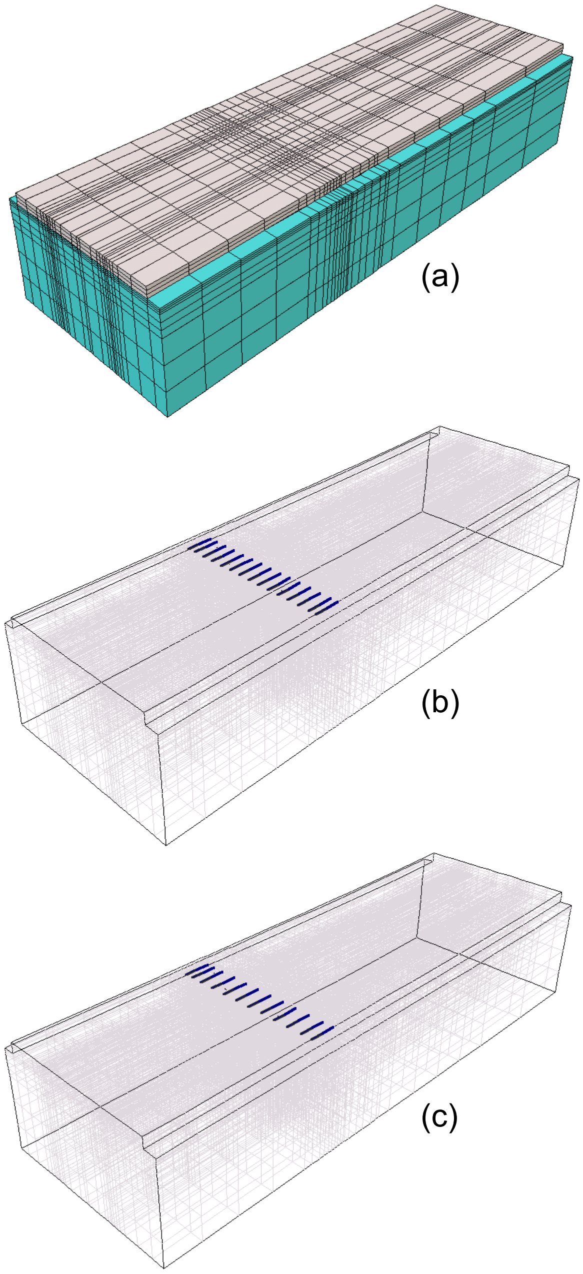

Figure 11 Mesh for Analysis of Actual Pavement; (a) Mesh; (b) Type 1 & 2; (c) Type 3 & 4

Table 2 Input Data for Analysis of Loading Tests on Actual Pavement

Item [Symbol]	Value	Item [Symbol]	Value
Elastic Modulus of Concrete [E_c]	30,000 MPa	Poisson's Ratio of Subbase [μ_g]	0.35
Poisson's Ratio of Concrete [μ_c]	0.15	Thickness of Subbase [h_g]	2,600 mm
Thickness of Concrete Slab [h_c]	280 mm	Diameter of Dowel Bar [ϕ]	28 and 32 mm
Elastic Modulus of Subbase [E_b]	1,000 MPa	Length of Dowel Bar [L_d]	700 mm
Poisson's Ratio of Subbase [μ_b]	0.35	Elastic Modulus of Dowel Bar [E_d]	210,000 MPa
Thickness of Subbase [h_b]	150 mm	Poisson's Ratio of Dowel Bar [μ_d]	0.3
Elastic Modulus of Subbase[E_g]	30 Mpa	Interaction Spring Constant between Dowel Bar andConcrete [K_c]	400 GN/m^3

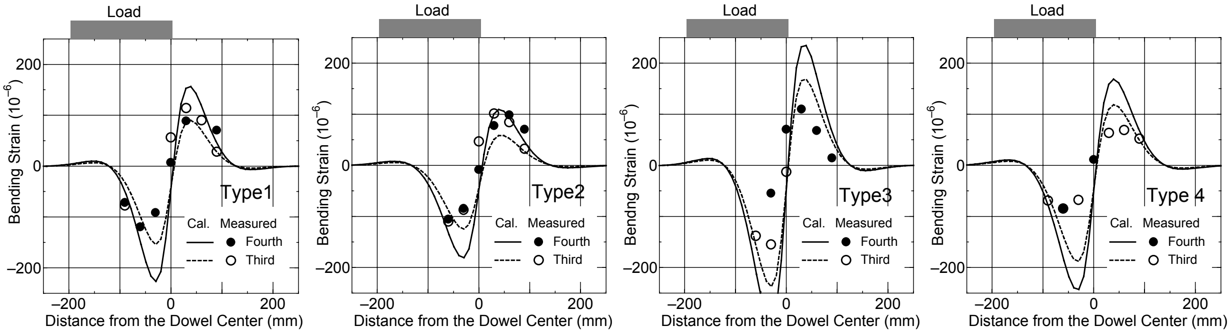

Figure 12 Strain Distributions in Dowel Bars in Actual Pavement

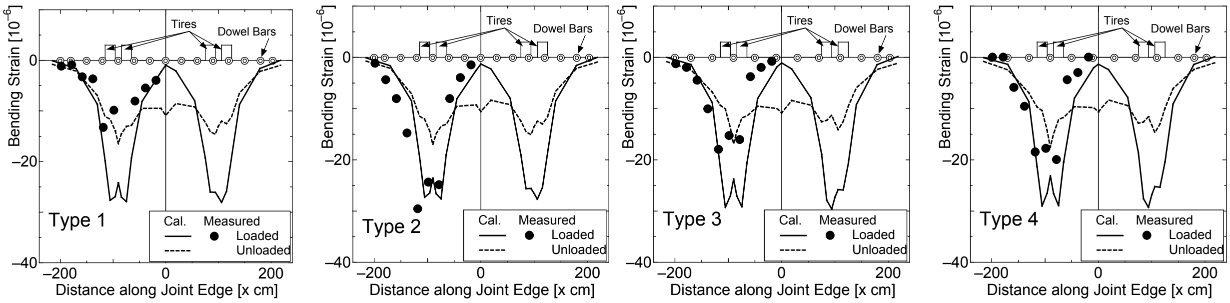

Figure 13 Strain Distributions in Concrete Slabs in Actual Pavement

Figure 12 shows the strain distributions in the dowel bars with strain gauges. Some of the strain gauges on the dowel bars failed, and only reliable data are plotted in the figure. Although the predicted strains overestimate the measured values, the agreement between predicted and measured results is fairly good from a practical point of view.

Figure 13 shows the strain distribution on the slab surface along the transverse joint. Although the predicted strains are larger than the measured values, the overall tendency is quite similar in both cases. From these results, it can be said that PVAE3D is a good tool for predicting the behavior of dowel bars as well as concrete slabs.

5. MECHANICAL BEHAVIOR OF TRANSVERSE JOINT

In this section, the effects of the geometry and spacing of dowel bars and of subbase rigidity on the mechanical behavior of concrete slabs and dowel bars are investigated with PAVE3D simulations. The simulations were performed on a concrete pavement with the transverse joint of Type 3 as a reference structure. The dowel bar length, value of K_c, joint opening width, L_b, and subbase stiffness, E_b, varied as presented in Table3. The joint opening width mentioned here is the length of the beam element and does not necessarily reflect the actual opening of the joint. If it is greater than the actual opening, the inner nodes are located not on the surface of the solid elements but within them, which means that the concrete support around the center of the dowel bar is lost.

Table 3 Parameter Values for Simulation

Item [Symbol]	Values
Elastic Modulus of Subbase [E_b]	500, 1,000, 10,000 MPa
Diameter of Dowel Bar [ϕ]	28, and 32 mm
Length of Unsupported Dowel Bar [L_b]	20, 40, and 60 mm
Length of Dowel Bar [L_d]	500, and 700 mm
Interaction Spring Constant between Dowel Bar and Concrete [K_c]	100, 200, and 400 GN/m^3

5.1 Dowel Bar Stress

Figure 14 shows the distributions of maximum bending stress in dowel bars along the joint edge. As the diameter of the dowel bar increases from 28 mm to 32 mm, the maximum stress decreases by about 25%. On the other hand, a 20% stress reduction is obtained by narrowing the dowel spacing from 400 mm to 300 mm.

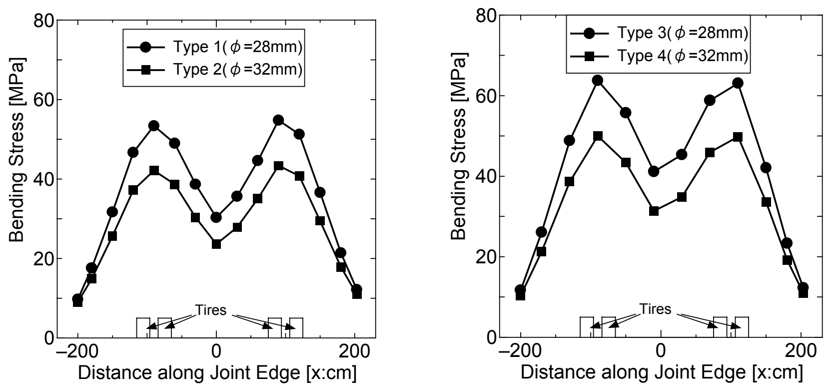

Figure 14 Maximum Bending Stresses of Dowel Bars along Joint Edge

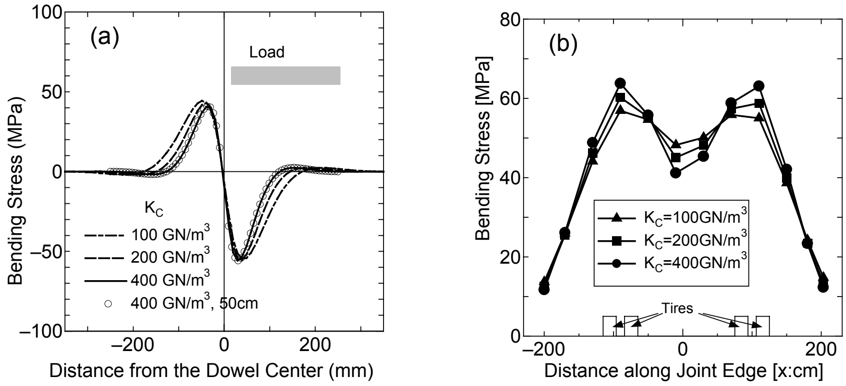

Figure 15 Effect of K_c on Bending Stress of Dowel Bar; (a) Stress Distribution in a Dowel Bar; (b) Stresses along Joint Edge

Figure 15 shows the effect of K_c on the bending stress in the dowel bars. As K_c increases, the range within which bending stress occurs is reduced and the magnitude of the maximum stress increases. Changing the dowel bar length from 700 mm (solid line in Figure 15(a)) to 500 mm (circle marks) has no effect on bending stress. From Figure 15(b), it is found that, if K_c = 400 GN/m^3, the bending stress of the dowel bar just under the tire is greater than when K_c = 100 GN/m^3 and the bending stresses in other dowel bars between the tires are smaller. So, if the concrete strongly restrains the dowel bars, the stresses in the dowel bars under the tires are large but those between the tires are relatively small.

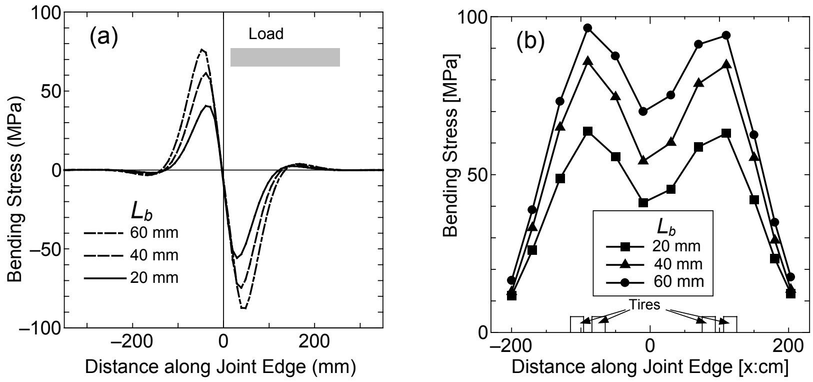

Figure 16 Effect of L_b on Bending Stress of Dowel Bar; (a) Stress Distribution in a Dowel Bar; (b) Stresses along Joint Edge

Figure 16 shows the effect of L_b on the bending stress in the dowel bars. Increasing L_b from 20 mm to 60 mm causes a rise in the bending stresses of all dowel bars by about 40%. Therefore, if the concrete around the dowel bar in the joint opening region were to weaken and ultimately fail to support the dowel there, the dowel bar stress would significantly increase.

Figure 17 shows the effect of E_b on the stress of the dowel bar. The magnitude of E_b varied from 500 MPa for a granular subbase to 10,000 MPa for a lean concrete subbase. Increasing E_b decreases the bending stresses in all dowel bars by about 20%.

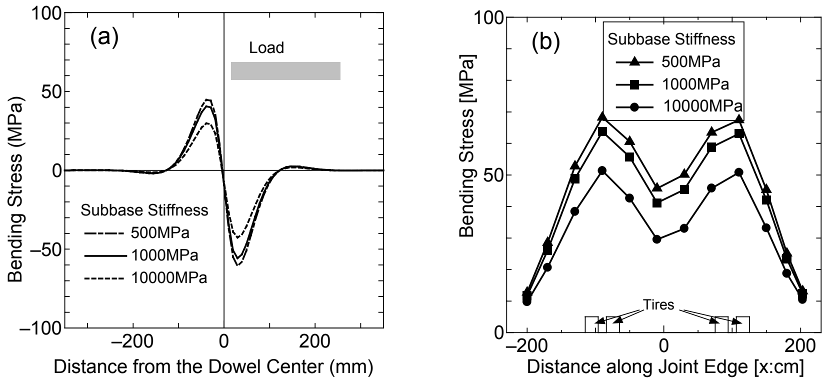

Figure 17 Effect of E_b on Bending Stress of Dowel Bar; (a) Stress Distribution in a Dowel Bar; (b) Stresses along Joint Edge

5.2 Concrete Slab Stresses

In this section, the bending stresses at the bottom of the concrete slab and the transfer efficiency across the transverse joint are discussed.

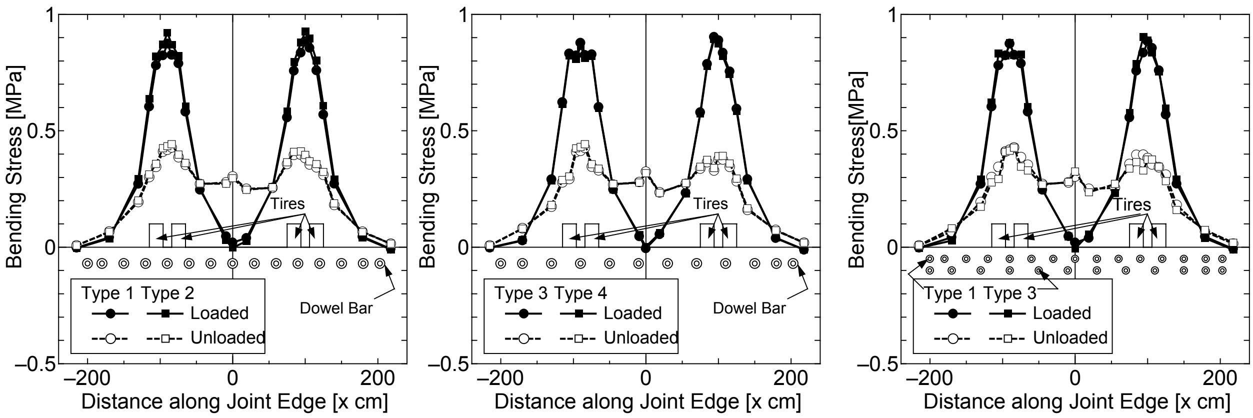

Figure 18 Bending Stress Distributions in Concrete Slab along Transverse Joint Edge

Figure 18 shows stress distributions along the transverse joint edge in loaded and unloaded slabs to allow comparison of the stresses for different joint types. Naturally, stresses in the loaded slab are greater immediately under the tires than in other parts of the slab. In the unloaded slab, relatively large stresses are observed in the position corresponding to the position between the tires in the loaded slab. This is because the load is carried by a number of dowel bars over quite a wide range of transverse distance. Further, from Figures 18(a) and (b), it can be said that increasing the dowel diameter from 28 mm to 32 mm has very little effect on concrete stresses. Figure 18(c) shows that there is no difference in stress for the two dowel spacings of 400 mm and 300 mm. Therefore, the joint types considered in this experiment have no significant effect on concrete stresses.

In this study, the load transfer efficiency expressed in deflection or stress is defined as follows:

$$e_{ff} = \frac{2s_2}{s_1 + s_2} \times 100 \qquad (20)$$

where,

e_{ff} = load transfer efficiency(%) and

s_1, s_2 = stresses or deflections of the loaded and unloaded slabs, respectively.

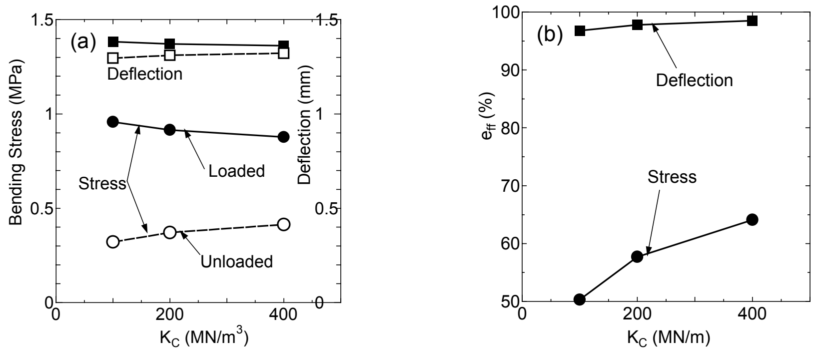

Figure 19 Effects of K_c on (a) Stress and Deflection and (b) Load Transfer Efficiencies

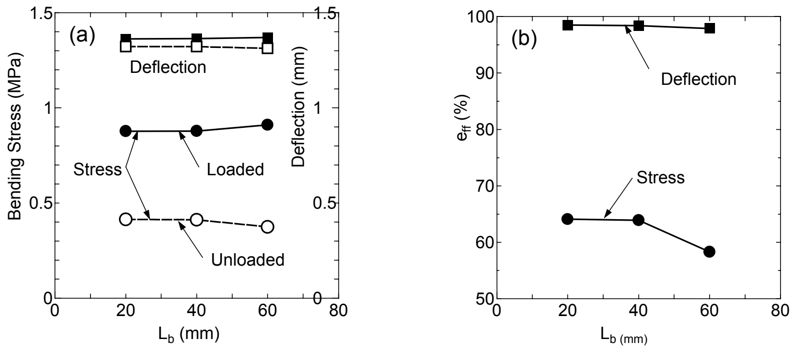

Figure 20 Effects of L_b on (a) Stress and Deflection and (b) Load Transfer Efficiencies

Figure 19 shows the effect of K_c on e_{ff}. An increase in K_c decreases the stress in the loaded slab and increases the stress in the unloaded slab, leading to higher e_{ff} in stress, while the effect of K_c on deflection is very little.

Figure 20 shows the effect of L_b on e_{ff}. For values of L_b less than 40 mm, the effect seems to be slight. When L_b rises above 60 mm, the stress and deflection increase in the loaded slab and decrease in the unloaded slab, leading to lower e_{ff}. In general practice, the joint opening width is 10 mm to 20 mm. In this range, there is likely to be no impact on concrete stresses, which means no reduction in the effectiveness of the dowel bar. However, if the concrete around the dowel bar becomes weak after repeated loading, the support provided to the dowel bar by the concrete will be lost and the unsupported length of the dowel bar may increase to 40 mm or more. This will lead to higher bending stresses in the concrete slabs.

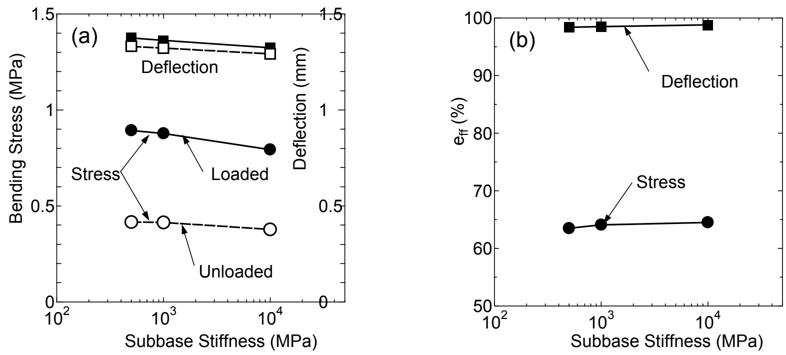

Figure 21 Effects of E_b on (a) Stress and Deflection and (b) Load Transfer Efficiencies

Figure 21 shows the effect of E_b on concrete stress. An increase in E_b reduces both the deflections and stresses of the loaded and unloaded slabs, though it has little effect on e_{ff}.This means that increasing the strength of the subbase might be a good means of improving the structural capacity of the overall pavement system under traffic loading.

6. CONCLUSION

In this study, a mechanical model for dowel bars in the transverse joints between concrete pavement slabs was developed based on the three-dimensional finite element method. In the model, a dowel bar is divided into three segments: two embedded in the concrete and a third linking them together. The embedded segments are modeled by solving for a beam on an elastic foundation while the joint segment is treated as a three-dimensional beam element. The resulting dowel bar element was formulated for a 3DFEM code, PAVE3D, which allows one to compute displacements and stresses of the dowel bar as well as those of the concrete slabs, subbase, and subgrade, taking into account the geometry and spacing of the dowel bar.

The model was verified by comparing predicted strains in the concrete slabs and dowel bars with experimental data obtained in loading tests conducted on a model pavement and also on an actual pavement. The comparison resulted in fairly good agreement, thus confirming the validity of PAVE3D.

The effects of transverse joint structure on stresses in dowel bars and concrete slabs were investigated by carrying out numerical simulations with PAVE3D. The results of these simulations showed that the geometry and spacing of dowel bars have great effect on stresses in the dowel bars, but the effect on concrete slab stresses is relatively small. It was also found that increasing the subbase rigidity decreases the stresses in both dowel bars and concrete slabs. Therefore, strengthening the subbase might be considered a good measure for enhancing the structural capacity of concrete pavement systems.

References

[1] *Manual for Portland Cement Concrete Pavement*, Japan Road Association, 1981 (in Japanese)

[2] Fukuda, T., Koyanagawa, M., and Murai, S., "Condition Survey of Concrete Pavements and Its Evaluation", *Proceedings of 3rd International Conference on Concrete Pavement Design and Rehabilitation*, Purdue University, pp.519-523, 1985

[3] Iijima, T., and Kubota, K., "Evaluation of Serviceability of Test Pavement in Yaita Bypass", *Proc. of JSCE*, No. 388/V-4, pp.65-74, 1980 (in Japanese)

[4] Tabatabaie, A.M., and Barenberg, E.J., "Finite Element Analysis of Jointed or Cracked Concrete Pavements", *Transportation Research Record 671*, Transportation Research Board, pp.11-17, 1978

[5] Huang, Y.H., and Chou, Y.T., "Discussion on Finite Element Analysis of Jointed or Cracked Pavements", *Transportation Research Record 671*, Transportation Research Board, pp.17-18, 1978

[6] Tayabiji, S.D., and Colley, B.E., "Analysis of Jointed Concrete Pavements", *FHWA-RD-86-041*, Turner-Fairbanks Highway Res. Ctr., McLean, Va., 1986

[7] Ioannides, A.M., "Analysis of Slab-on-grade for a Variety of Loading and Support Conditions", PhD thesis, University of Illinois, Urbana, Ill., 1984

[8] Fukute, T., Hachiya, Y., and Yamazaki, H., "Load Transfer Function across Joint in Concrete Pavement", *Report of Port and Harbor Research Institute*, Ministry of Transportation, Vol.21, No.2, pp.207-236, 1982 (in Japanese)

[9] Nishizawa, T., Fukuda, T., and Matsuno, S., "Analysis of Mechanical Behavior of Transverse Joint in Concrete Pavement", *Proc. of JSCE*, No.378/V-6, pp.185-193, 1987 (in Japanese)

[10] Nishizawa, T., Fukuda, T., and Matsuno, S., "A Refined Model of Doweled Joints for Concrete Pavement Using FEM", *Proceedings of 4th International Conference on Concrete Pavement Design and Rehabilitation*, Purdue University, pp. 735-745, 1989

[11] Guo, H., Sherwood, J.S., and Snyder, M.B., "Component Dowel-Bar Model for Load Transfer Systems in PCC Pavements", *Journal of Transportation Engineering*, ASCE, Vol. 121, No. 3, pp.289-298, 1995

[12] *Proceedings of National Symposium on 3D Finite Element Modeling for Pavement Analysis, Design, and Research*, Charleston, West Virginia, 1998

[13] *Proceedings of 2nd International Symposium on 3D Finite Element for Pavement Analysis, Design, and Research*, Charleston, West Virginia, 2000

[14] Shoukry, S.N., and William, G., "3D FEM Analysis of Load Transfer Efficiency", *Proceedings of National Symposium on 3D Finite Element Modeling for Pavement Analysis, Design, and Research*, Charleston, West Virginia, pp.40-50, 1998

[15] Davids, W.G., and Mahoney, J.P., "Experimental Verification of Rigid Pavement Joint Load Transfer Modeling with EverFE", *Transportation Research Record 1684*, Transportation Research Board, pp. 81-89, 1998

[16] Zienkievicz, O.C., *The Finite Element Method*, Third Edition, McGraw-Hill, Inc., 1977

[17] Nishizawa, T., Development of 3D FEM Program Package for Structural Analysis of Pavement System, *Journal of Pavement Engineering*, JSCE, Vol.5, 2000 (in Japanese) (http://www.plan.civil.tohoku.ac.jp/pave/hoso-ml/download.html)

[18] Przemienieki, J.K., *Theory of Matrix Structural Analysis*, McGraw-Hill, Inc., p.79, 1968

[19] Yorder, E.J., and Witczak, M.W., *Principle of Pavement Design*, Second Edition, John Wiley and Sons, Inc., New York, p.99, 1975